CT and MR Imaging of Nitinol Stents with Radiopaque Distal Markers

Laurent Létourneau-Guillon, Gilles Soulez, MD, MSc, Gilles Beaudoin, PhD, Vincent L. Oliva, MD, Marie-France Giroux, MD, Zhao Qin, MSc, Nicolas Boussion, PhD, Éric Therasse, MD, Jacques de Guise, PhD, and Guy Cloutier, PhD

PURPOSE: To evaluate imaging characteristics and artifacts of a nitinol stent with distal tantalum markers with computed tomography (CT) angiography and magnetic resonance (MR) angiography.

MATERIALS AND METHODS: A vascular phantom was built to simulate in-stent restenosis. A nitinol stent with tantalum markers (Luminexx stent) was evaluated with CT angiography in different orientations relative to the z-axis and with MR angiography in different positions relative to both B0 and the readout gradient. Stenosis measurements were compared with conventional digital subtraction angiography for both modalities. In-stent signal intensity obtained with different flip angles was assessed in two nitinol stents with distal markers (Luminexx stent and SMART stent) and one without markers (Memotherm-FLEXX stent).

RESULTS: Stenosis detection was not possible with CT angiography when the stent was perpendicular to the z-axis because of streak-like artifacts induced by tantalum markers. Stenosis evaluation with multiplanar reformation was accurate when the stent was in parallel and oblique orientations relative to the table axis. With MR angiography, metallic artifacts were mostly related to the stent orientation with B0, whereas orientation of the readout gradient had little influence. The mean error (overestimation) for stenosis measurements varied between 0.1% and 7.4% for CT imaging in parallel and oblique positions and 3.6% and 9.5% for MR imaging. Higher flip angles did not improve signal intensity inside the three stents tested.

CONCLUSION: CT and MR angiography can be used for evaluating the patency of stents with distal markers that are parallel or oblique relative to the table axis (iliac, carotid, or femoral stents). MR angiography is preferred if the stent is perpendicular to the table axis (renal stent).

J Vasc Interv Radiol 2004; 15:615–624

Abbreviations: FOV = field of view, MPR = multiplanar reformations, RF = radiofrequency

VASCULAR stents are now widely used in peripheral revascularization. There is a need for follow-up vascular imaging after stent placement in peripheral vessels to detect in-stent restenosis caused by thrombus formation or neointimal hyperplasia (1). Intra-arterial digital subtraction angiography (DSA) is the gold standard procedure to image in-stent restenosis. However, this technique is invasive and requires the use of nephrotoxic contrast agent and ionizing radiation. Direct visualization of iliac vessels by color Doppler ultrasound (US) is often limited by bowel gas interposition and can be difficult in obese patients. Computed tomography (CT) angiography also uses iodinated contrast material and ionizing radiation but is noninvasive. Because of its high longitudinal and temporal resolution, multidetector CT allows reliable CT angiography of iliac arteries (2). Stent imaging with CT is afflicted by artificial narrowing of the in-stent lumen and beam hardening artifacts, which may hamper restenosis assessment (3–5). In addition, metallic artifacts are more pronounced in stents with tantalum markers compared with nitinol stents without markers (4,5). The accuracy of CT angiography to detect in-stent stenosis has not been well established because of the limited number of patients with such occurrence in available clinical series (3,6). Contrast-enhanced three-dimensional magnetic resonance (MR) angiography now offers an alternative to x-ray angiography in different vascular territories (7–9). However, MR imaging of vascular stents is limited by susceptibility and radiofrequency (RF) shielding artifacts related to the metallic composition of the stent (10,11). In general, stents made of nitinol or tantalum alloy induce less artifacts than cobalt and stainless steel stents (12,13). Because nitinol stents have a low radiopacity, fluoroscopic

From the Department of Radiology (L.L.G. [Medical Student], G.S., G.B., V.L.O., M.F.G., E.T.), Laboratory of Biorheology and Medical Ultrasonics-Research Center (Z.Q., N.B., G.C.), Laboratory of Orthopedic Imaging-Research Center (J.d.G.), CHUM–Notre-Dame Hospital, 1560 Sherbrooke East, Montreal, Quebec, Canada, H2L 4M1. From the 2003 SIR annual meeting. Received January 11, 2004; revision requested February 3; revision received Feburary 18; accepted February 19. **Address correspondence to** G.S.; E-mail: gilles.soulez.chum@ssss.gouv.qc.ca

Supported in part by grants from the Canadian Institute of Health Research (G.C., G.S., #MOP-53244) and Valorisation-Recherche Québec (group grant #2200–094); by a research studentship (L.L.G.) and scholarships (G.C., G.S.) from the Fonds de la Recherche en Santé du Québec; and in-kind support (stents) from Bard Medical–Angiomed.

None of the authors has identified a potential conflict of interest.

DOI: 10.1097/01.RVI.00000127898.23424.01

visualization can be improved by placing distal opaque markers at the stent extremities.

The purpose of this study was to assess the accuracy of CT and MR imaging for evaluating in-stent restenosis of a nitinol stent with tantalum markers. For that purpose, a multimodality realistic phantom model of in stent restenosis was used.

MATERIALS AND METHODS

Phantom Model of In-Stent Double Stenosis

A dedicated multimodality vascular phantom was designed for the study (14,15). It was based on a modified version of a phantom used to evaluate the geometric accuracy of x-ray angiography, CT angiography, MR angiography and ultrasound. An 8-mm-diameter, 60-mm-long Luminexx stent (Bard Medical–Angiomed, Karlsruhe, Germany) was placed horizontally between the inlet and outlet of the phantom. The Luminex (Bard-Angiomed) stent is a nitinol vascular stent with the same geometry as the Memotherm-FLEXX stent (Bard Medical–Angiomed) but with the addition of tantalum markers at its extremities to facilitate fluroscopic visualization. Mild and moderate stenoses were created in the stent by insertion of a low melting point cerrolow rod within the stent. This cerrolow rod had the shape of the narrowed vessel lumen and it was covered by a thin layer of latex. After positioning of the rod, the phantom of polyethylene was filled with an agar solidified gel that simulated the imaging texture of human tissues. Cerrolow, which has a low fusion temperature of 55° C, was removed after heating the phantom in hot water, leaving the stent with two in-stent stenoses respectively of 30% and 50% diameter reduction. Both stenoses were covered by an inner layer of latex to prevent contrast diffusion within the gel. This assembly was embedded in the agar block and connected to tubes at the extremities of the phantom to allow injection of contrast media.

X-ray Angiography

A single acquisition was done in AP projection (field of view [FOV], 17 cm; tube to image intensifier distance, 82 cm; table height, 105 cm; matrix size: 512 × 512, 25 mA, 60 kV) on a HICOR/ACOM-TOP angiographic unit (Siemens, Erlangen, Germany). This small FOV was chosen to obtain the same pixel size as with a DSA unit with 1,024 × 1,024 matrix size and a FOV of 33 or 40 cm. A graduated catheter was taped on the outside of the phantom at the same level as the simulated vessel to allow calibration. The vascular phantom was filled with a solution of 300 mg/mL of iothalamate meglumine (Conray 30; Mallinckrodt Medical, Pointe-Claire, Quebec, Canada). This iodine concentration was chosen because it allowed reproduction of an opacification of the vascular lumen similar to intra-arterial injection during catheter angiography. The phantom was then pressurized to 100 mm Hg to allow latex vessel expansion and close fitting to the agar gel vessel lumen.

CT Angiography

The phantom was filled with a 2.8% solution of 430 mg/mL of iothalamate meglumine (Conray 43; Mallinckrodt Medical, Pointe-Claire, Quebec, Canada) diluted with a 0.9% NaCl solution. This concentration was used to simulate the contrast obtained after bolus injection during CT angiography. This gave an average attenuation of 207 HU ± 21 on a background of 48 HU ± 2. The phantom was then pressurized to 100 mm Hg. It was scanned with a PQ5000 CT scanner (Philips Medical Systems, Best, The Netherlands) with slice thickness of 1 mm, pitch of 1.25, and reconstruction interval of 1 mm. A technique of 200 mA and 120 kVp was used for all scans. Three scans were obtained successively with the phantom oriented parallel, 45 degrees obliquely and perpendicularly to the z-axis (table axis). The phantom was always placed in the center of the gantry. To cover the phantom length, FOV of 16, 20, and 25 cm were used for the parallel, oblique and perpendicular orientations, respectively. Small FOV were chosen to maximize spatial resolution.

MR Angiography

MR imaging was performed with a 1.5-T MR unit (Magnetom Vision; Siemens, Erlangen, Germany). The phantom vessel was filled with a 1.8 mmol/L gadopentetate dimeglumine solution (Magnevist; Berlex Canada, Lachine, Quebec, Canada) diluted with 0.9% NaCl solution (to reproduce the signal intensity observed in gadolinium-enhanced MR angiography) and then pressurized to 100 mm Hg. A high resolution three-dimensional fast low angle shot sequence was used in the coronal plane with a body array coil (repetition time, 4.6 msec; echo time, 1.8 msec; flip angle, 30°; FOV, 293 × 390 mm; matrix size, 300 × 512; slab thickness, 60 mm; effective slice thickness, 1.67 mm; 50% overlap reconstructions; number excitation, 1). A larger FOV was used for MR compared with CT because in a clinical setting, it is not possible to decrease the FOV without inducing a wrap artifact. Series were obtained with the vascular phantom oriented parallel and then perpendicular to the main magnetic field (B0). For each of these orientations to B0, the readout gradient (frequency encoding axis) was positioned parallel and perpendicular to the stent, which gave a total of four series.

A second experiment was performed to study the effect of tantalum markers on artifact production and to assess in-stent signal intensity changes with flip angle variation. Three different nitinol stents (one with tantalum markers, one without distal markers, and one with gold markers) were placed on nylon wires into a water bath filled with the same concentration of gadopentetate dimeglumine as the one used for the vascular phantom experiment. The three stents were, respectively, a 10-mm-diameter, 60-mm-long Luminexx stent (Bard Medical–Angiomed), a 10-mm-diameter, 50-mm-long Memotherm-FLEXX stent (Bard-Angiomed), and a 10-mm-diameter, 80-mm-long SMART stent (Cordis, Miami, FL). With the same MR angiography sequence previously described, the acquisitions were performed with stents oriented parallel to both the main magnetic field and the readout gradient with flip angles of 30°, 60°, 90°, 120°, and 150°.

Image Analysis

Source images, coronal and sagittal multiplanar reformations (MPR) (slice thickness, 2 mm) were examined for

data sets obtained with CT, whereas source images and maximum intensity projections were reviewed for MR series. Each CT and MR series was analyzed with special attention to occurrence of artifacts and visibility of the stent lumen. This evaluation was performed independently by one investigator (G.S.) who was not involved in the processing of diameter measurements. The following artifact scoring system was used: 0, no artifact and optimal lumen delineation; 1, minor artifacts not impairing lumen assessment; 2, moderate artifacts slightly impairing delineation of the inner lumen; 3, severe artifacts interfering with lumen delineation; 4, major artifacts obscuring the stent margin and stented lumen (4). Diameter measurements were performed with the use of a public domain software (Image J, version 1.27z, National Institutes of Health, Bethesda, MD). All but one diameter measurement were calculated quantitatively with a full-width at half maximum/minimum approach, which allowed window setting-independent measurements (12). It was not possible to use this software to measure the diameter of the mild stenosis in CT angiography when the stent was in oblique orientation because artificial enlargement of stent struts interfered with the assessment of the vessel border. This measurement was thus performed manually with electronic calipers.

Stenosis Evaluation

The maximum diameter reductions of both in-stent stenoses and reference diameters outside the stent were measured for each CT and MR acquisition. Stenosis percentage calculations were performed as follows:

$$\frac{\text{non-stented vessel diameter} - \text{stenosis diameter}}{\text{non-stented vessel diameter}} \times 100$$

The reference diameter of the mild stenosis was measured proximal to the stent, whereas the reference diameter of the moderate stenosis was measured distal to the stent. These measurements were repeated in four different sessions by the same observer. For CT angiography, diameter measurements were obtained from the axial source images for the series with the phantom parallel to the table axis. MPR were used to obtain cross-sectional images for the two series with the phantom oriented obliquely and perpendicularly to the z-axis. For MR series, subvolume targeted maximum intensity projections in the coronal plane were used for diameter measurements. For analysis of both CT angiography and MR angiography series, stenosis percentage of the four consecutive measurements made in each series were averaged and compared with angiographic measurements.

Evaluation of MR stent artifacts.—Quantitative evaluation of MR stent-induced artifacts (lumen narrowing, spiky artifacts along the lumen) was done by measuring 10 random values of the lumen diameter at the center of the stent (between the stenoses). Mean diameter and SD were calculated. Percentage of in-stent lumen reduction compared with the x-ray angiography was also calculated.

CT attenuation evaluation.—CT source images were also evaluated for changes in attenuation values inside the stent compared with the vessel outside the stent. Fifteen random measurements of the lumen attenuation values inside and outside the stent were done for all CT series with regions of interest drawn into the vessel lumen with use of the eFilm software (eFilm Medical, Toronto, ON). In these measurements, the mean attenuation value was used for analysis.

In-stent signal and flip angle.—Evaluation of signal inside the stent with flip angle variation was made with the gadolinium water bath experience. For each flip angle, signal intensity was measured for regions of interest drawn inside and outside the stent lumen.

Statistical Analysis

Stenosis diameters and percentages calculated from CT and MR were compared with the results of x-ray angiography with a two-tailed paired Student *t* test on Excel software. HU measurements with CT and MR signal intensities were also compared with a Student *t* test.

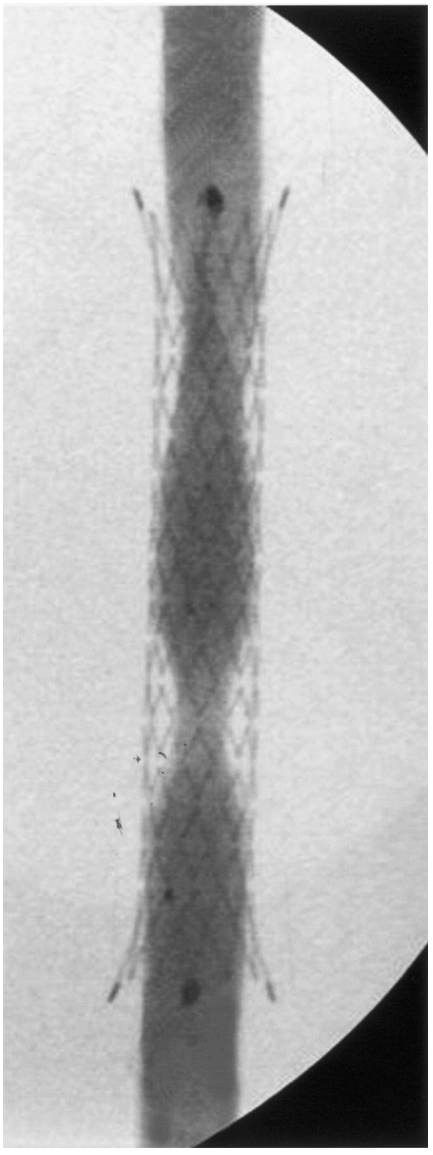

Figure 1. Angiography of the vascular phantom filled with iodinated contrast medium. The two concentric stenoses are well demonstrated. Tantalum markers are seen even with contrast material superposition.

RESULTS

Angiography and Stenosis Evaluation

The phantom vessel was well depicted on x-ray angiography and tantalum markers were visualized even with iodinated contrast material superimposition (**Fig 1**). The stenosis percentages measured at angiography were 31.5% and 48.8%, which is close to the expected values of 30% and 50%, respectively. Absolute errors of

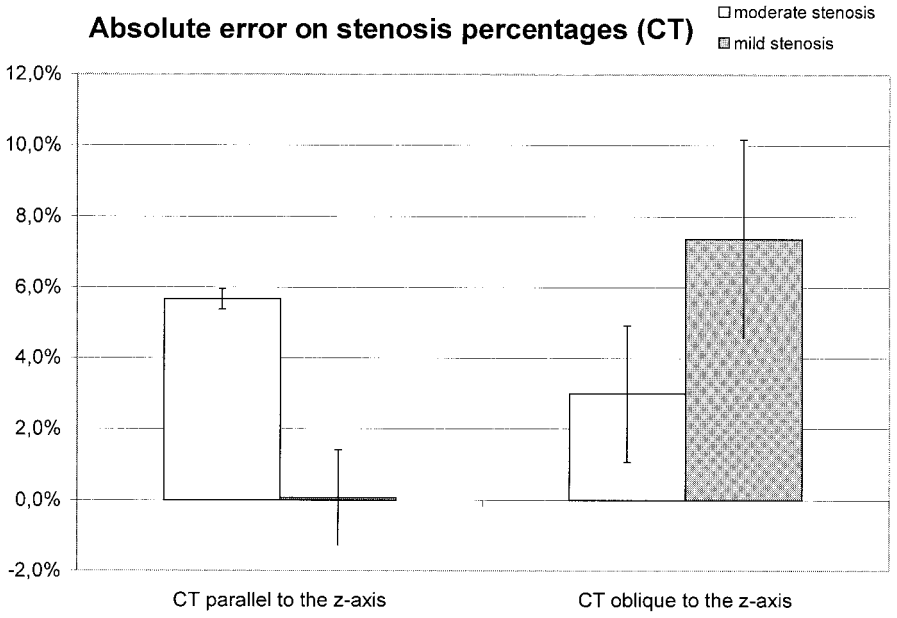

Figure 2. Absolute errors on stenoses percentages in CT angiography. No measurement has been performed with the stent perpendicular to the z-axis because of the presence of streak-like artifacts. Note that stenosis diameter measurement of the mild stenosis in the oblique orientation was performed manually.

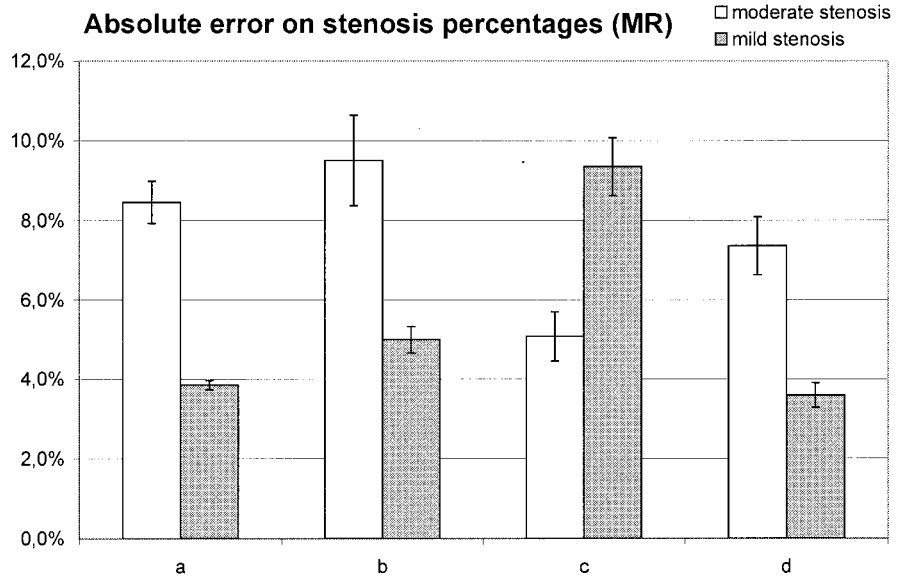

Figure 3. Absolute errors on stenoses percentages. **(a)** MR parallel to B0 and parallel to the readout gradient. **(b)** MR parallel to B0 and perpendicular to the readout gradient. **(c)** MR perpendicular to B0 and perpendicular to the readout gradient. **(d)** MR perpendicular to B0 and parallel to the readout gradient.

stenoses percentage evaluation for CT and MR are summarized graphically in **Figs 2, 3**. **Table 1** summarizes artifact scores, and stenoses percentages for each acquisition with the different modalities.

CT Angiography

The stent lumen was visible when the phantom was oriented parallel and oblique to the z-axis (**Fig 4a**). The nitinol struts were clearly seen in axial sections but were enlarged compared with x-ray angiography. The strut thickness measured 0.51 ± 0.01 mm at angiography compared with 1.02 ± 0.03 mm when the stent was parallel to the table axis with CT ($P < .01$) and 2.96 ± 0.60 mm ($P < .01$) when the stent was positioned obliquely on the table. On source images, there were no severe metallic artifacts along the length of the nitinol stent except at the level of tantalum markers, which produced severe streak-like artifacts (**Fig 4a**). Coronal or sagittal MPRs allowed partial compensation for this effect. The perpendicular orientation to the z-axis did not permit an adequate assessment of the in-stent lumen because of severe beam-hardening artifacts (**Fig 4b**).

All reference diameters were slightly but significantly overestimated (range, 0.36–0.66 mm; relative error range, 4.8%–8.6%). Luminal diameter measurements inside the moderate stenosis were slightly but significantly underestimated when the stent was in parallel orientation, (0.26 mm underestimation; relative error, −7.4%). Luminal diameter measurements of the mild stenosis were overestimated when the phantom was oriented parallel to the z-axis (0.47 mm overestimation; relative error, 8.8%). Overestimation of stenosis percentages varied between 0.1% and 7.4%. This overestimation was significant for the moderate stenosis when the stent was in parallel orientation (5.7% overestimation; relative error, 10.3%) and for the mild stenosis when it was in oblique orientation (7.4% overestimation; relative error, 19%).

Attenuation values in the vessel lumen inside and outside the stent lumen did not vary significantly for the parallel (227 HU ± 7 versus 223 HU ± 6; $P = .0516$) and oblique (188 HU ± 8 versus 190 HU ± 10, $P = .7457$) orientations to the table axis. When the stent was oriented perpendicular to the z-axis, severe artifacts induced important variation of attenuation values inside and outside the stent lumen (114 ± 20 versus 72 ± 45; range, 36.65–155.67 HU; $P = .007$).

MR Angiography

Figure 5 illustrates the four series obtained with MR imaging. Overall, the stent lumen was easily delineated. The perpendicular orientation to the

Table 1
Stenoses Percentage Measurements Observed on Angiography, CT Angiography, and MR Angiography*

Modality	Artifact Scoring	Moderate Stenosis (50% diameter reduction)	Mild Stenosis (30% diameter reduction)
X-ray angiography	0	49.2 ± 1.1%	31.5 ± 0.2%
CT Angiography			
Stent parallel to the z-axis	1	54.9 ± 0.3% ($P<.05$)	31.6 ± 1.3% ($P=.921$)
Stent oblique to the z-axis	2	52.2 ± 1.9% ($P=.12$)	38.9 ± 2.8%† ($P<.05$)
Stent perpendicular to the z-axis	4	Measurements were not possible due to severe artifacts	
MR Angiography			
Stent parallel to B0 and the readout	2	57.7 ± 0.5% ($P<.05$)	35.4 ± 0.1% ($P<.05$)
Stent parallel to B0 and perpendicular to the readout	2	58.7 ± 1.1% ($P<.05$)	36.5 ± 0.3% $P<.05$)
Stent perpendicular to B0 and perpendicular to the readout	3	54.3 ± 0.6% ($P<.05$)	40.9 ± 0.7% ($P<.05$)
Stent perpendicular to B0 and parallel to the readout	2	56.6 ± 0.7% ($P<.05$)	35.1 ± 0.3% ($P<.05$)

* The statistical comparisons were performed with the measurements on x-ray angiography.
† The stenosis diameter was measured using a manual technique and the reference diameter with a quantification software.

main magnetic field clearly narrowed the in-stent lumen diameter and decreased the depiction of the mild stenosis (**Fig 5c, d**). In fact, diameter measurements taken at the center of the stent showed a reduction in the lumen diameter (**Table 2**), especially when the stent was perpendicular to B0. The orientation to the readout gradient had a less dramatic consequence on artifact production and essentially changed the shape of these artifacts. A spiky pattern appearance was observed along the lumen when the stent was parallel to the readout gradient (**Fig 5a, d**). This phenomenon explained the increase in SD of the lumen diameter measurements at the center of the stent (**Table 2**).

On MR angiography, all reference diameters measured outside the stent were overestimated by a mean of 0.66 mm (range, 0.40–0.91 mm; relative error range, 5.2%–11.4%). Underestimation of the lumen inside the moderate stenosis was observed in the four series (mean, 0.37 mm; range, 0.21–0.44 mm; relative error range, −5.9 to −13.6%). Measurements of the mild stenosis diameter were slightly but significantly underestimated (mean, 0.23 mm; relative error, −5.0%) for the experiments with the phantom perpendicular to both the main magnetic field and the readout gradient, whereas it was slightly but significantly overestimated for the three other MR series (mean, 0.26 mm; range, 0.22–0.29 mm; relative error range, 4.4%–5.7%). Calculated stenosis percentages were slightly but significantly overestimated for both the moderate stenosis (mean, 7.6%; range, 5.1–9.5%; relative error range, 9.4%–16.2%) and the mild stenosis (mean, 5.4%; range, 3.6%–9.3%; relative error range, 10.2%–22.9%).

Effect of Distal Markers and Flip Angles

Figure 6 shows the different series obtained with the stents immersed in the gadopentetate-dimeglumine solution. **Figure 7** plots flip angles and signal intensities for the three stents and the gadolinium solution. With increasing flip angles, a decrease of in-stent and background signal intensity was observed for the three stents. This experimentation allowed us to compare the artifacts induced by the extremities of the three stents. Tantalum markers produced slightly larger signal voids than both the unmarked nitinol extremities of the Memotherm-FLEXX stent (Bard Medical–Angiomed) and the gold markers of the SMART stent (Cordis). However, marker-related artifacts did not interfere with the lumen diameter evaluation.

DISCUSSION

Phantom Model

Only one study by Maintz et al (16) evaluated in vitro imaging of eccentric in-stent stenosis with wax pieces to mimic stenoses. Our phantom is more anthropomorphic than the one suggested by Maintz et al (16) and has the advantage of concentric stenosis. With the method used in this study, it is possible to simulate realistic stenosis derived from clinical angiographic findings. The lost casting material technique uses a low melting point metal rod mimicking the inner lumen of the vessel. This rod was thermically removed to create the vessel lumen in the phantom. With this lost-material casting technique, the angiographic

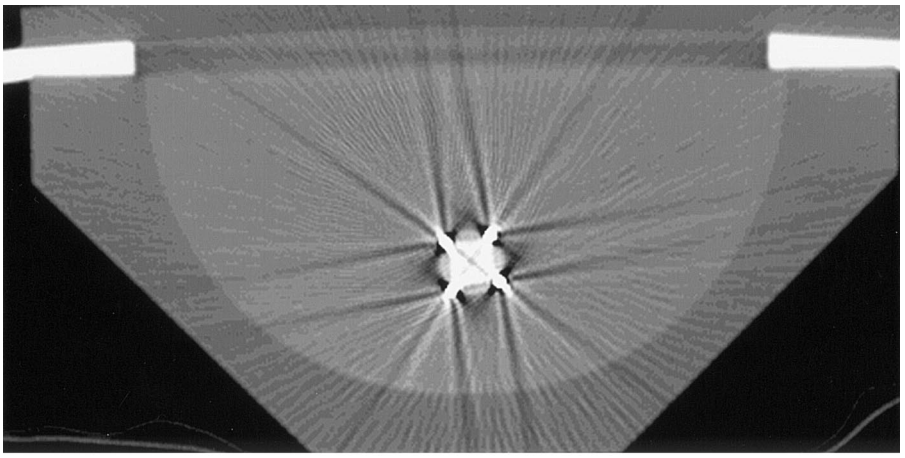

a.

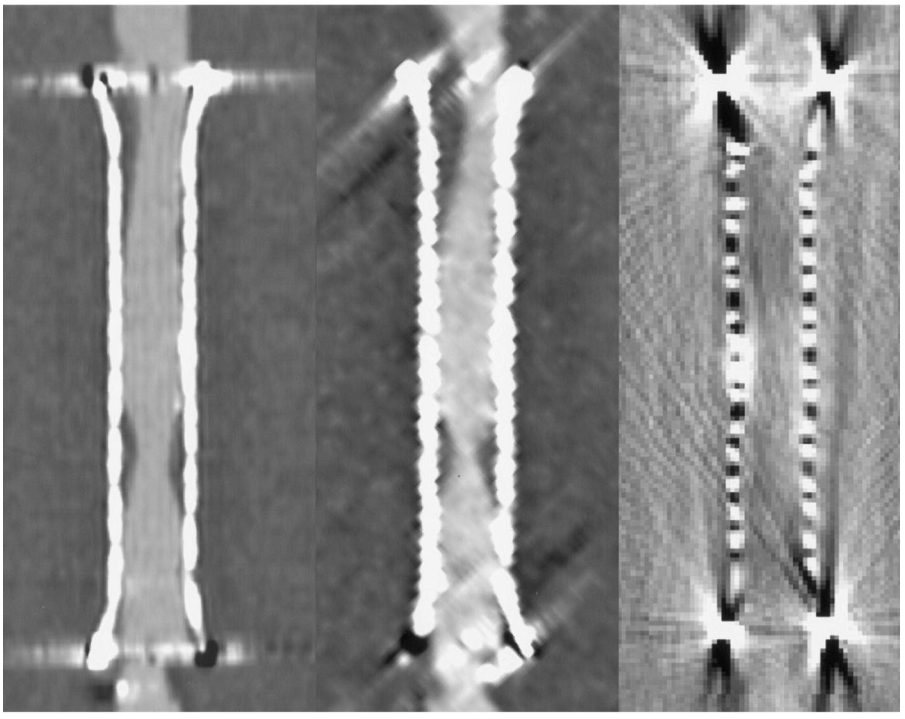

b.

Figure 4. **(a)** CT scan axial section (source images) through the tantalum markers with the phantom oriented parallel to the z-axis. Severe streak artifacts obscure the lumen of the stent. **(b)** Coronal MPR of CT imaging acquisitions with the phantom oriented parallel (left), oblique (middle), and perpendicular to the z-axis (right). Note that coronal MPR reduces the magnitude of the streak artifacts. A thickening of the stent wall is observed when the stent is oblique to the z-axis impairing the delineation of the mild stenosis. The stent lumen cannot be analyzed when the stent is perpendicular to the z-axis.

measurements were close to the expected degree of stenosis. These findings confirm the accuracy and precision of this technique (15). In this study, angiographic measurements were used as the gold standard as it is the case in clinical practice.

CT Angiography

This study shows that stenosis detection with CT angiography is possible in stents with distal markers if they are not oriented perpendicularly to the z-axis. With multidetector CT technology, it is now possible to decrease slice thickness and acquisition time, and to improve spatial resolution. This improved longitudinal spatial resolution allows high resolution MPRs, which provide a better evaluation of in-stent stenosis. Maintz et al (16) compared MR angiography and multiple-slice CT imaging of 10 stents and concluded that multiple-slice CT imaging offered superior lumen visualization compared with MR angiography in all but one tantalum stent tested. In their study, stenosis evaluation was performed qualitatively with a 5-point scale. The model of in-stent stenosis used in their study was less realistic and precise than the current model. In addition, there was no evaluation of the influence of the stent orientation on artifacts production and stenosis evaluation. In this study, the addition of radiopaque tantalum markers was the principal cause of artifact production and image quality degradation in CT. Others researchers found that platinum or gold markers induced similar artifacts with other stents (4,16). The streak-like artifacts induced by tantalum can be explained by the high radiopacity of this material. The Strecker tantalum stent (Boston Scientific, Natick, MA) induced the most artifacts with CT compared with other commercially available metallic endovascular devices (4,5). Nevertheless, MPR in coronal and sagittal planes decreased the magnitude of these artifacts and allowed a better visualization of the inner and outer margins of the stent at the level of tantalum markers. Fishman et al (17) already used this simple imaging method to overcome metallic artifacts arising from metallic hip implants.

The stent lumen could not be analyzed when the stent was perpendicular to the z-axis. Similarly, Wise et al (18) observed with a carotid artery phantom that acquisition with the phantom oriented perpendicularly to the z-axis yielded a significantly higher number of false-occlusions compared with other orientations because of beam-hardening. Because no stent was used in their experimentation, the opacity of the column of contrast medium was sufficient to induce beam hardening. In this study, beam-hardening was probably induced by tantalum markers. Recently, Behar et al (3) reported a good correlation be-

Table 2
Lumen Diameter at the Center of the Stent (without Stenosis) Measured in MR Angiography

	Diameter (mm)			SD (mm)	Relative Error (%)
	Maximum	Mean	Minimum		
Parallel to both B0 and the readout gradient	8.2	7.1	6.2	0.60	0.5
Parallel to B0 and perpendicular to the readout gradient	7.1	6.8	6.5	0.21	−3.3
Perpendicular to both B0 and the readout gradients	5.8	5.5	5.2	0.21	−21.5
Perpendicular to B0 and parallel to the readout gradient	6.3	5.9	5.3	0.33	−16.3

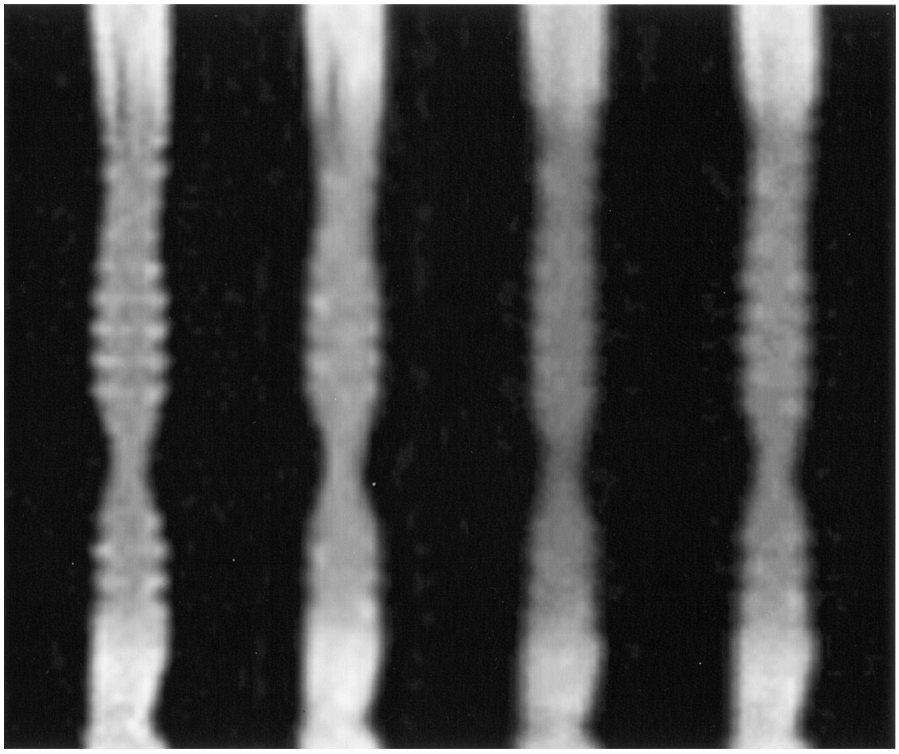

a. **b.** **c.** **d.**

Figure 5. Maximum intensity projections from the MR angiography acquisition of the vascular phantom displayed with the same window setting. **(a)** Stent parallel to B0 and parallel to the readout gradient. **(b)** Stent parallel to B0 and perpendicular to the readout gradient. **(c)** Stent perpendicular to B0 and perpendicular to the readout gradient, **(d)** Stent perpendicular to B0 and parallel to the readout gradient. Both stenoses are well depicted on the first two series with the stent parallel to Bo **(a,b)**. When the stent is oriented perpendicular to the main magnetic field **(c,d)**, the narrowing of the stent lumen hampers the assessment of the mild stenosis. A spiky pattern is observed when the stent is positioned parallel to the readout gradient **(a,d)** This pattern is less marked when the stent is oriented perpendicular to the readout gradient **(b,c)**.

tween CT angiography and angiography in stented renal arteries. Renal arteries are oriented perpendicular to the z-axis and, in this study, balloon expandable stents without distal markers were used.

The slight overestimation of stenosis evaluation was related to the following: i) underestimation of the stenosis lumen for the moderate stenosis and ii) overestimation of the reference diameter for both stenoses. However, the stenosis percentage overestimation was less than 10%, which should not be problematic in most clinical situations. Other researchers have found systematic underestimation of luminal diameters in stents (3,4). This underestimation was less pronounced for nitinol stents (5). Underestimation of stent lumen can be explained by apparent thickening of the stent wall with CT. Similar artificial thickening has also been reported with various other endovascular devices (4–6). This artificial thickening of the stent wall may be a result of volume averaging and would consequently increase with an orientation of the stent perpendicular or oblique to the z-axis because of a lower longitudinal spatial resolution (6). Addis et al (19) found that both source axial projection images and coronal and sagittal MPRs had a tendency to underestimate minimal luminal diameters of stenoses greater than 50% but to accurately depict the minimal luminal diameter of mild stenosis. This phenomenon may explain the fact that in this study, for most acquisitions, the moderate stenosis was more overestimated than the mild one.

This study used small FOV (16–25 cm) to maximize spatial resolution. To reproduce these results in a clinical setting, a high resolution CT acquisition with a small FOV centered on the stent area should be performed. This is supported by the results obtained by Behar et al (3). In this series, detection of in-stent restenosis in the renal arteries was achieved with use of 20 cm FOV, a detector configuration of 4.0 × 1.25 mm, and image reconstruction with thickness of 1.25 mm (3).

MR Angiography

Thorough understanding of stent-related artifacts is of key importance for optimizing stent imaging with MR. Such knowledge recently lead Buecker

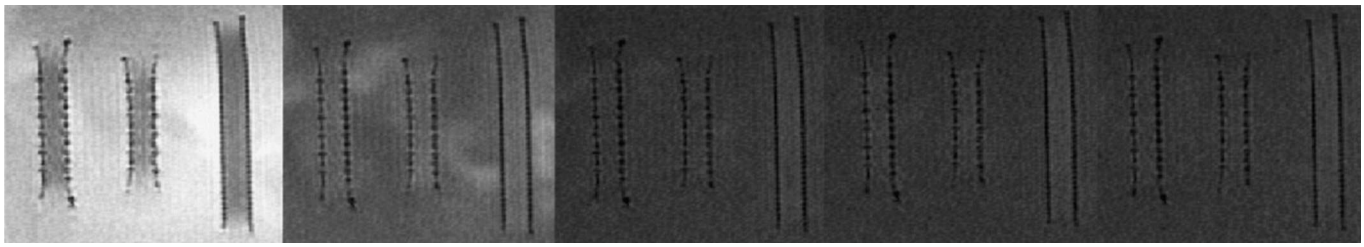

Figure 6. Coronal source images of MR angiography with increasing flip angles (30°, 60°, 90°, 120°, 150°) at the same window level and width (WL: 420; WW: 920). An overall decrease of signal intensity in the stent and the background is observed with the increasing flip angle.

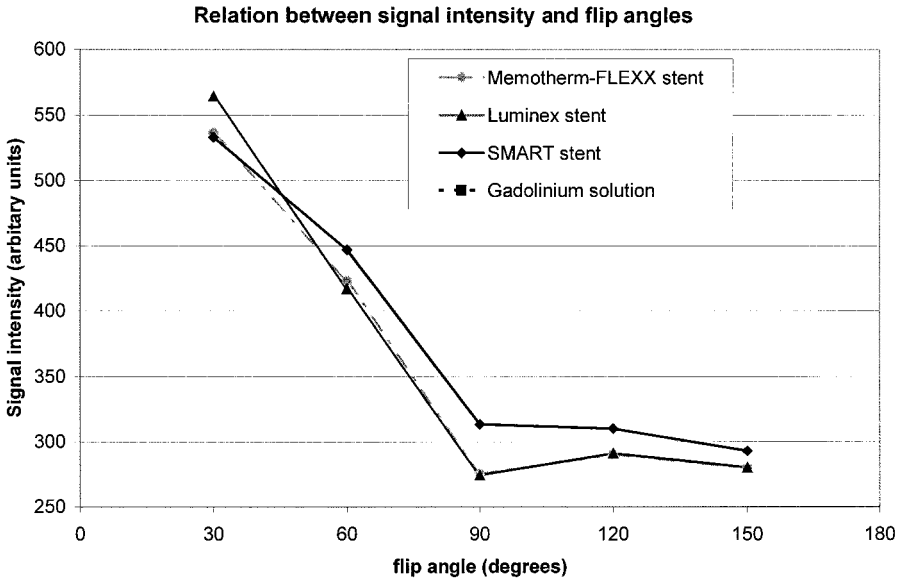

Figure 7. Changes in signal intensities with increasing flip angle. An overall reduction in signal intensity was observed.

et al (20) to design an artifact-free stent of woven copper with wide filament spacing. Unfortunately, this stent was only of theoretical interest because it lacked radial force. Several factors influence stent artifact production in MR. Magnetic field strength, echo time, and orientation of the stent to both the main magnetic field and the readout and sequence types are among the main factors influencing susceptibility artifact production (10,12,13,21). Stent composition also influences susceptibility artifacts with greater effect arising from stainless steel and cobalt-based alloy stents than from nitinol or tantalum stents (10–13,22). Stent design is also an important factor to consider. For example, Meyer et al (12) found that one stainless steel stent offered better lumen visibility than many nitinol stents because of its design. Moreover, Maintz et al (10) found differences in in-stent signal homogeneity between nitinol stents. Artifact production in stents made of nitinol arises from RF shielding artifacts that decrease the amplitude of the transmitted RF pulse inside stents while shielding the signal emitted by spins located inside the device (23).

In this study, the in-stent lumen was well depicted in all series on MR angiography sequences with high spatial resolution (in-plane pixel size, 0.76 × 0.98 mm). However, there was noticeable narrowing of the in-stent lumen with the stent oriented perpendicular to the main magnetic field. In fact, the latter orientation has been shown to be the source of signal loss at the level of the stent wall (12,21). The shape of stent-related artifacts is also influenced by the direction of the frequency encoding gradient, as also reported with other stent types (10,13,21). It was observed in the current study that a spiky pattern corresponding to the stent geometry was influenced by this encoding gradient.

In this study, overestimation of stenoses occurred in all MR sequences, but it was always less than 10%. The use of maximum intensity projections as the postprocessing algorithm may be responsible for this effect, or at least it may have exaggerated the trend toward stenosis overestimation in MR angiography (24,25). The use of volume rendering might have minimized this overestimation (25). Variations in diameter measurements were observed between the different orientations used, which may reflect differences in distortion of the lumen wall by artifacts induced by the stent struts. This effect was visible on the mild stenosis but did not affect the moderate stenosis, as shown in **Figure 5**.

One way to overcome RF shielding artifacts is to use a higher flip angle, which should produce an optimal flip angle inside the stent (23,26). It was decided in the current study to compare the Luminex stent to the SMART (Cordis) and Memotherm-FLEXX stents (Bard Medical–Angiomed) because improved lumen visualization has already been reported using higher flip angles for the latter two stents (23,26). In this study, paradoxically, an increase of the flip angle resulted in an overall signal intensity reduction inside the three stents and in the background. This can be explained by the use of a shorter repetition time (repetition time; 4.6 versus 17–22 msec). Indeed, if a short repetition time and echo time are used, an increase of the flip angle will not affect

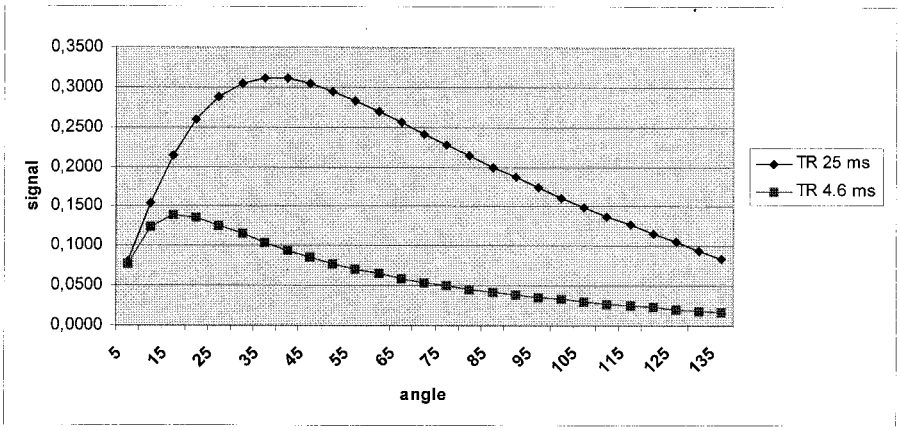

Figure 8. Calculation of signal intensity as a function of flip angle for repetition time values at 25 msec and 4.6 msec.

in-stent signal. This can be easily demonstrated by estimating the signal intensity proportionally to the magnetization transfer as a function of the excitation angle, echo time, repetition time and both relaxation times T1 and T2 as reported by Bartels et al (23). As shown in **Figure 8**, the theoretical variation of signal intensity of diluted gadolinium as a function of flip angle for repetition time and echo time values used in previous reports was compared with the values used in this study (23,26).

This study observed slightly larger artifacts with Tantalum markers compared with the unmarked ends of the Memotherm-FLEXX stent (Bard Medical–Angiomed). Surprisingly, Tantalum by itself produces few susceptibility artifacts as shown with the Strecker tantalum stent in other studies (10,13). As such, the artifacts observed in this study could be caused by the increased thickness of the stent at the level of these Tantalum markers compared with the free ends of unmarked stents. In the current study, the artifacts induced by distal markers did not interfere with vessel lumen analysis.

In a clinical setting, it can be hypothesized that the use of a short repetition time and echo time gradient-echo MR angiography sequence with a high spatial resolution is appropriate to image in-stent stenosis. In the particular case of a nitinol stent with distal markers, orientation of the stent perpendicular to the table axis will have a less deleterious effect on image quality compared with CT acquisition.

Limitations

The effects of flow and pulsatility were not evaluated in this study. CT detects only differences in radiopacity and is insensitive to flow. Conversely, MR could be affected by intravoxel dephasing with a flow phantom. Nevertheless, Maintz et al (10) compared the results obtained with their static model with the results obtained by Hilfiker et al (27) on a circulating phantom and found artifact patterns to be similar for one stent.

Another potential shortcoming of this study is the absence of stenosis directly at the level of the end markers. In the model in this study, stenoses were intentionally created within the stents to simulate in-stent restenosis as it is most commonly seen clinically. In case of a stenosis located at the edge of the stent within the tantalum markers, a more pronounced deterioration of measurement reliability could have been observed, especially with CT.

CONCLUSIONS

With use of high resolution acquisitions, both CT angiography and MR angiography allowed adequate evaluation of in-stent lumen with the exception of a perpendicular stent orientation relative to the z-axis with CT imaging. Stenosis measurements were similar for both modalities with slight overestimation (less than 10%) of in-stent stenosis. There was no improvement of in-stent MR signal with flip angle increase when short repetition time sequence was used. In conclusion, it is believed that both modalities are adequate for stent imaging despite the presence of distal markers for imaging of iliac, femoral, or carotid stents. Situations in which the stent is oriented perpendicular to the table axis (renal stent) should be evaluated with MR because of severe artifacts induced by distal markers with CT imaging.

References

1. Vorwerk D, Gunther R, Schurman K, et al. Aortic and iliac stenoses: follow-up results of stent placement after insufficient ballon angioplasty in 118 cases. Radiology 1996; 198:45–48.
2. Rubin GD, Shiau MC, Leung AN, Kee ST, Logan LJ, Sofilos MC. Aorta and iliac arteries: single versus multiple detector-row helical CT angiography. Radiology 2000; 215:670–676.
3. Behar JV, Nelson RC, Zidar JP, DeLOng DM, Smith TP. Thin-section multidetector angiography of renal artery stents. AJR Am J Roentgenol 2002; 178:1155–1159.
4. Maintz D, Fischvach R, Juergens KU, Allkemper T, Wessling J, Heinidel W. Multislice CT angiography of the iliac arteries in the presence of various stents: In vitro evaluation of artifacts and lumen visibility. Invest Radiol 2001; 12:699–704.
5. Strotzer M, Lenhart M, Butz B, Völk M, Manke C, Feuerbach S. Apperance of vascular stents in computed tomographic angiography: in vitro examination of 14 different stent types. Invest Radiol 2001; 11:652–658.
6. Chopra S, Ghiatas AA, Encarnacion CE, et al. Transjugular intrahepatic portosystemic shunts: assessment with helical CT angiography. Radiology 1997; 202:277–280.
7. Reimer P, Landwehr P. Non-invasive vascular imaging of peripheral vessels. Eur Radiol 1998; 8:858–872.
8. Quinn SF, Sheley RC, Semonsen KG, Leonardo VJ, Kojima K, Szumowski J. Aortic and lower-extremiy arterial disease: evaluation with MR angiography versus conventional angiography. Radiology 1998; 206:693–701.
9. Prince MR, Narasimham DL, Stanley JC, et al. Breath-hold gadolinium-enhanced MR angiography of the abdominal aorta and its major branches. Radiology 1995; 197:785–792.
10. Maintz D, Kugel H, Schellhammer F, Landwehr P. In vitro evaluation of intravascular stent artifacts in three-di-

mensional MR angiography. Invest Radiol 2001; 36:218–224.
11. Link J, Steffens JC, Brossmann J, Graessner J, Hackethal S, Heller M. Iliofemoral arterial occlusive disease: contrast-enhanced MR angiography for preinterventional evaluation and follow-up after stent placement. Radiology 1999; 212:371–377.
12. Meyer JMA, Buecker A, Schuermann K, Ruebben A, Guenther RW. MR evaluation of stent patency: in vitro tests of 22 metallic stents and the possibility of determining their patency by MR angiography. Invest Radiol 2000; 12:739–746.
13. Lenhardt M, Volk M, Manke C, et al. Stent appearance at contrast-enhanced MR angiography: in vitro examination with 14 stents. Radiology 2000; 217:173–178.
14. Teppaz P, Qanadli S, Cloutier G, Soulez G, Cimon R, Durand LG. Multimodality vascular imaging phantom and process for manufacturing said phantom. US and international patent pending, 2001.
15. Cloutier G, Soulez G, Teppaz P, Qanadli SD, Qin Z, Durand LG. A multimodality vascular imaging phantom for calibration purpose. In Galloway Jr, RL, ed. Medical imaging. Volume 5029, Visualization, image-guided procedure, and display, proceedings of SPIE. SPIE-the international Society for optical engineering: Bellingham, Washington, 2003;707–716.
16. Maintz D, Tombach B, Juergens KU, Weigel S, Heindel W, Fischbach R. Revealing in-stent stenoses of the iliac arteries: comparison of multidetector CT with MR angiography and digital radiographic angiography in a phantom model. AJR Am J Roentgenol 2002; 179:1319–1322.
17. Fishman EK, Magid D, Robertson DD, Brooker AF, Weiss P, Siegelman SS. Metallic hip implants: CT with multiplanar reconstruction. Radiology 1986; 160:675–681.
18. Wise SW, Hopper KD, Ten Have T, Schwartz T. Measuring carotid artery stenosis using CT angiography: the dilemma of artifactual lumen eccentricity. AJR Am J Roentgenol 1998; 173: 919–923.
19. Addis KA, Hopper KD, Iyriboz TA, Liu Y, Wise SW, Kasales CJ. CT angiography: in vitro comparison of five reconstruction methods. AJR Am J Roentgenol 2001; 177:1771–1776.
20. Buecker A, Spuentrup E, Ruebben A, Gunther RW. Artifact-free in-stent visualization by standard magnetic resonance angiography using a new metallic magnetic resonance imaging stent. Circulation 2002; 105:1772–1775.
21. Klemm T, Duda S, Machann J, et al. MR imaging in the presence of vascular stents: A systematic assessment of artifacts for various stents orientations, sequence types and field strenghts. J Magn Reson Imaging 2000; 12:606–615.
22. Shellock FG, Shellock VJ. Metallic stents: evaluation of MR imaging safety. AJR Am J Roentgenol 1999; 173: 543–547.
23. Bartels LW, Bakker CJG, Viergever MA. Improved lumen visualization in metallic vascular implants by reducing RF artifacts. Magn Reson Med 2002; 47:171–180.
24. Lee VS, Martin DJ, Krinsky GA, Rofsky NM. Gadolinium-enhanced MR angiography: artifacts and pitfalls. AJR Am J Roentgenol 2000; 175:197–205.
25. Baskaran V, Pereles FS, Nemcek AA, et al. Gadolinium-enhanced 3D MR angiography of renal artery stenosis: a pilot comparison of maximum intensity projection, multiplanar reformatting, and 3D volume-rendering postprocessing algorithms. Acad Radiol 2002; 9:50–59.
26. Meyer JMA, Buecker A, Spuentrup E, et al. Improved in-stent magnetic resonance angiography with high flip angle excitation. Invest Radiol 2001; 36: 677–681.
27. Hilfiker PR, Quick HH, Pfammatter T, Schmidt M, Debatin JF. Three-dimensional MR angiography of a nitinol-based abdominal aortic stent-graft: assessment of heating and imaging characteristics at three-dimensional MR angiography. Radiology 1999; 211: 693–697.